2020 IEEE/RSJ International Conference on Intelligent Robots and Systems (IROS)
October 25-29, 2020, Las Vegas, NV, USA (Virtual)

Three-Dimensional Posture Optimization for Biped Robot Stepping over Large Ditch Based on a Ducted-Fan Propulsion System

Zhifeng Huang, *Member, IEEE*, Zijun Wang, Jiapeng Wei, Jingtao Yu, Yuhao Zhou, Pihao Lao, Xiaoliang Huang, Xuexi Zhang, and Yun Zhang[a], *Member, IEEE*

***Abstract*—The recent progress of an ongoing project utilizing a ducted-fan propulsion system to improve a humanoid robot's ability to step over large ditches is reported. A novel method (GAS) based on the genetic algorithm with smoothness constraint can effectively minimize the thrust by optimizing the robot's posture during 3D stepping. The significant advantage of the method is that it can realize the continuity and smoothness of the thrust and pelvis trajectories. The method enables the landing point of the robot's swing foot to be not only in the forward but also in a side direction. The methods were evaluated by simulation and by being applied on a prototype robot, Jet-HR1. By keeping a quasistatic balance, the robot could step over a ditch with a span of 450 mm (as much as 97% of the length of the robot's leg) in 3D stepping.**

I. Introduction

Stepping over large obstacles and ditches is considered an indispensable ability for a humanoid robot to carry out tasks in an extreme environment, such as one with earthquake debris and a rough terrain. In such a situation, the scattered obstacles and fragile surfaces are considered the main challenge for robots. The former might cause the available landing points to be scattered. In other words, the robot needs to locate its feet in a side direction rather than a forward direction. As a result, 3D stepping for robots over large ditches or obstacles is necessary. Meanwhile, the other challenge, fragile terrains, might limit the robot when it performs a dynamic motion over an obstacle, such as jumping. For such situations, the robot should be able to maintain quasistatic balance, even though its center of mass (CoM) is out of the support polygon when the swing leg is extended. In view of this, it is important to develop a new method to help the robot overcome these two challenges.

For the problem of stepping over an obstacle while keeping balance, many methods have been proposed. Kalamian et al. used a nonlinear model predictive control method, and a robot succeeded in stepping over a 40- × 15-cm obstacle in a simulation [1]. Zhou et al. enlarged the workplace of a humanoid robot by exploiting the redundancy of the pelvis rotation. This method was proved effective by having a robot step over an obstacle whose height was 100 mm, 20% of its leg, and whose width was 50 mm [2]. Guo et al. proposed a method that enables a robot to step over two large obstacles continuously [3]. Robert et al. used a new A* footstep planner that realized stepping over rough terrain in the real world with Atlas [4]. Another idea is that a humanoid robot can keep balance by itself with a multicontact method, but it needs surfaces in an environment [5] [6]. Most of the methods above focused on stepping over high, but not wide, obstacles. Methods of multicontacting were more feasible. However, reliable supporting points might be scarce in real environments. In addition, because the upper limbs are occupied, the executable task of the humanoid is restricted.

Recently, because the performance of brushless motors has significantly improved, a rotor propulsion system with a high thrust-to-weight ratio (up to 10) has become possible. Some researchers have started focusing on applying aerodynamic lift to improve the performance of traditional robots. Zhao et al. developed a dragonlike aerial robot based on a ducted fan. The robot can transform in the air to fly across a narrow space [7]. Endo et al. utilized a thruster to compensate for the gravity of a superlong manipulator [8]. Moreover, researchers at IIT have begun a new project involving a flying humanoid, focusing on the control strategy for the stabilization of the robot [9]. The methods above were suitable for a robot completely hovering in the air or with one side fixed on the ground, but they might not be suitable for a humanoid robot in stepping.

In previous work [10], a prototype robot, Jet-HR1, was proposed with a ducted fan installed on its feet. Utilizing the proposed sliding gait and the method of posture optimization based on sequential quadratic programming, the robot could step over a ditch with a width of as much as 97% of the robot's leg length. However, the method was only for 2D gaits. which required a landing point to be located at the right forward of the robot.

In this study, to improve further the flexibility of the robot in stepping, a method was developed to optimize the robot's posture during 3D stepping. The aim of the method was to enable the robot to step over a ditch as wide as possible with limited thrust and keeping the quasistatic balance. The main challenges are as follows.

- The relationship between the feasible posture and the thrust needed to balance the capsizing moment of gravity was highly nonlinear. Moreover, the redundant degrees of freedom (DoFs) further increased the difficulty of the optimization.

[a]Corresponding author: Y. Zhang { yz@gdut.edu.cn, }
Research supported by the National Natural Science Foundation of China (NSFC) (Grant No. 51605098 and U1501251) and Natural Science Foundation of Guangdong Province, China (Grant No. 2016A030310350).

Z. Huang et al. are associated with the School of Automation, Guangdong University of Technology, Guangzhou 510006, P. R. China. {zhifeng@gdut.edu.cn}

X. Huang was with the Department of Electrical Engineering, Chalmers University of Technology (e-mail: xiaoliang.huang@ieee.org).

- To stabilize the robot motion during stepping, the trajectory of the robot joints and needed thrust should both be smooth. In other words, the minimization of the thrust should involve a careful tradeoff.

To overcome the challenges, first, the quasistatic balance model of the biped robot in 3D was simplified based on an analysis. Utilizing several preconditions by insight, the posture optimization, which was related to the positions of 12 joints, was converted into the problem of searching for the optimal position of the center of the robot's pelvis. Then, the model constraints were designed, and the genetic algorithm (GA) was applied to optimizing the robot's posture for minimizing the needed thrust. The smoothness of the motion and trajectory of thrust were also included in the proposed model constraints.

The main contributions of this work are (a) the improvement of the robot's hardware, including the new arrangement of the ducted-fan system and the gear mechanism to improve the torque of the roll axis of the joints, and (b) a new method of 3D posture optimization to minimize the thrust needed during stepping.

In this work, Section II is an introduction to the configuration of the hardware. In Section III, the 3D motion model in quasistatic balance is introduced, as well as the solution to the problem by using the GA with the designed constraint conditions and its implementation details. Section IV contains the results of the simulation and experiment. In Section V, the discussion and conclusions are provided.

II. Specification of Hardware Design

The prototype robot Jet-HR1 is shown in Fig. 1, and detailed specifications of the robot are listed in Table 1. Being different from the previous version [10], the new carbon fiber gear mechanism (Fig.1) was designed and installed in the hip

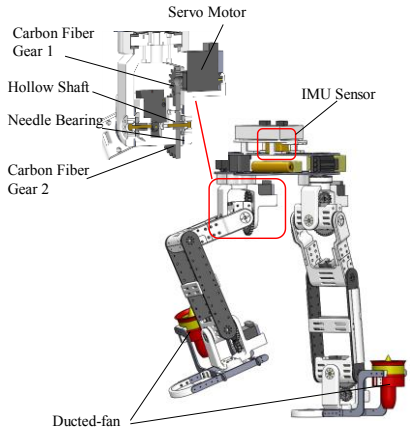

Figure 1. Improved version of Jet-HR1.

and ankle roll joints, to improve the robot's ability to step over a ditch in 3D stepping. The rest of the joints were driven by dual servo motors, except the hip joint in the yaw axis. In addition, the ducted-fan location was changed to be on the side of the feet. The new location provides the benefit of extending the force arm to balance the capsizing moment of gravity in the side direction.

TABLE 1

Main Specification

Component	Description
Weight	6.8 kg
Height	608 mm
Degrees of freedom	12
Length of leg	460 mm
Ducted fan	70 mm, 24 V, 232 g
	Max thrust 23 N @ 70 A
Joint servo motor	Kodon Kagaku. Co. Ltd. B3M1117, 12 V, 7.8 Nm
Carbon fiber gear ratio	1:2.43
Battery of servo motor	11.2 V, 2600 mAh

To measure the attitude of the robot's pelvis for feedback control, a six-axis inertia measurement unit (IMU), INS550, ASENSING Co., Ltd., was installed on the pelvis of the robot (Fig. 1).

III. Methods

In this section, the general quasistatic balance model of the robot in 3D stepping is analyzed first. Then. the problem of posture optimization is formulated, and its constraint condition is analyzed based on hardware, stability, and realizability. Finally, the GA is introduced, and the details of the implementation for applying it to the problem are provided.

A. General Model of Quasistatic Balance in 3D

The quasistatic balance model of the robot in 3D stepping is shown in Fig. 2. During quasistatic balance, the robot was assumed to move slowly, and the inertia force resulting from the velocity and acceleration was small and omitted. As a result, during stepping in 3D, there were only three types of force loading on the robot: gravity, thrust, and the supporting force of the ground. In this model, the ground was assumed to be horizontal, while the thrust was assumed to be vertical for the purpose of maximizing the ability to balance the gravity moment. According to the assumption

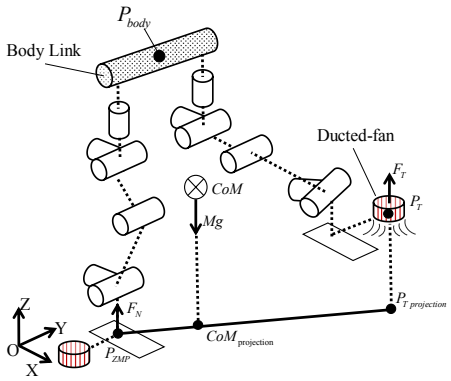

Figure 2. Quasistatic balance model in 3D.

above, to maintain the robot in balance, two rules should be kept: (1) the thrust and supporting force should be equal to the gravity and (2) the ground projection line from thrust to the position of the CoM ($\boldsymbol{CoM}$) of the robot should be across the support polygon of the support foot.

The rules above can be determined by the zero moment point (ZMP) theory and formulated as follows.

$$\boldsymbol{P}_{ZMP-X} = \frac{Mg \cdot \boldsymbol{CoM}_x - \boldsymbol{F}_{T-Z} \cdot \boldsymbol{P}_{T-X}}{Mg - \boldsymbol{F}_{T-Z}} \quad (1)$$

$$\boldsymbol{P}_{ZMP-Y} = \frac{Mg \cdot \boldsymbol{CoM}_y - \boldsymbol{F}_{T-Z} \cdot \boldsymbol{P}_{T-Y}}{Mg - \boldsymbol{F}_{T-Z}} \quad (2)$$

$$\boldsymbol{P}_{ZMP-Z} = 0 \quad (3)$$

where [$\boldsymbol{P}_{\text{ZMP-X}}$, $\boldsymbol{P}_{\text{ZMP-Y}}$, $\boldsymbol{P}_{\text{ZMP-Z}}$] is the position of the ZMP and should be located inside the support polygon of the support foot. $\boldsymbol{P}_{T\text{-}X}$ and $\boldsymbol{P}_{T\text{-}Y}$ are the positions of the ducted fan in the *X*- and *Y*-axes, respectively. The $\boldsymbol{CoM}$ of the robot was calculated by forward kinematics [11]. The highly nonlinear relationship between posture and thrust resulted from the $\boldsymbol{CoM}$ formulated by many trigonometric functions.

B. Precondition and Problem Simplification

The problem can be formulated as searching for the optimal posture to enable the robot to use the minimum thrust to keep balance when the swing foot is located in an assigned position in the air. The problem was somewhat similar to that of a redundant robot arm except for the ZMP constraint. Directly optimizing the robot's joint position might be unrealistic, because the highly redundant DoFs can consume considerable time. As a result, several preconditions were established to simplify the problem.

- Precondition 1. To extend the horizontal range in which swing feet can reach, the attitude of the body link (Fig. 3) must be parallel to the horizontal plane. The roll and pitch angles of the body link, α_{body} and β_{body}, should be zero. The yaw angle γ_{body} can be computed by the following equation.

$$\gamma_{body} = \tan^{-1}\left(\frac{P_{T-Y} - P_{ZMP-Y}}{P_{T-X} - P_{ZMP-X}}\right) \quad (4)$$

- Precondition 2. The attitude of the swing foot should stay parallel to the horizontal plane. Its attitude in the horizontal plane was required to remain forward for enlarging the range of the swing foot.

Precondition 2 is mainly for making the maximum use of the ducted-fan force for balancing the gravity. In addition, Precondition 2 makes it possible to avoid the ducted-fan thrust that would produce extra torque, which might cause the robot to rotate.

Utilizing the preconditions, the problem of posture optimization is further converted to optimize the position of the pelvis of the robot, which is located on the midpoint of the body link (Fig. 2). This point is ($\boldsymbol{P}_{body} \in \mathbb{R}^3$), as in the following section. Once the position of the pelvis has been determined, the angles of 12 joints can be calculated by inverse kinematics with the preconditions.

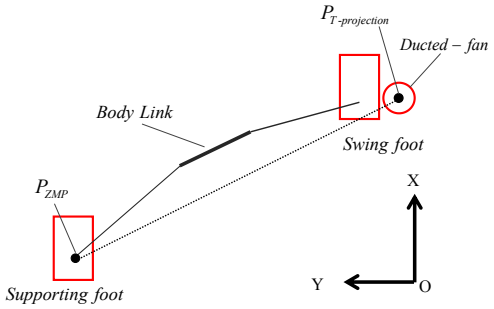

Figure 3. Simple model for Precondition 1.

C. Problem Modeling

As described above, the task was changed to finding the P_{body} that can minimize the force of the ducted fan and satisfy constraint conditions. The trajectory of the swing foot was predetermined and then discretized into limited points. The optimization should consider not only the current position of the swing foot, but also its previous position. To better express the problem, let $H(\cdot)$ be the nonlinear function that can compute $\boldsymbol{F}_{T-Z}$ with input $\boldsymbol{P}_{body}$ according to Eqs. (1)–(3) in the given $\boldsymbol{P}_{ZMP}$ and $\boldsymbol{P}_T$. One can consider this problem as a searching problem that can be described as follows.

$$\min_{\boldsymbol{P}_{body}} H(\boldsymbol{P}_{body}) \quad (5)$$

The constraint conditions are as follows.

$$\boldsymbol{R}_{body} = \boldsymbol{R}_{body}(\gamma_{body}) \in \mathbb{R}^{3\times3} \quad (6)$$

$$\boldsymbol{R}_{feet} = \boldsymbol{E} \in \mathbb{R}^{3\times3} \quad (7)$$

$$\boldsymbol{\theta}_{lb} \le \boldsymbol{\theta} \le \boldsymbol{\theta}_{ub}, \boldsymbol{\theta}_{lb} \text{ and } \boldsymbol{\theta}_{ub} \in \mathbb{R}^{12\times1} \quad (8)$$

$$0 \le F_{T-Z} \le F_{max} \quad (9)$$

$$|\theta_{ZC} - \theta_{CA}| \le \rho \quad (10)$$

$$\boldsymbol{P}_{ZMP} = [\boldsymbol{P}^1_{ZMP}, \dots, \boldsymbol{P}^N_{ZMP}] \in \{S_{foot}\} \quad (11)$$

$$\boldsymbol{P}_T = [\boldsymbol{P}^1_T, \dots, \boldsymbol{P}^N_T] \quad (12)$$

$$\left\|\boldsymbol{P}^N_{body}, \dots, \boldsymbol{P}^{N-1}_{body}\right\|^2_2 \le \delta \quad (13)$$

where $\boldsymbol{R}_{link}(\alpha, \beta, \gamma)$ represents the rotation matrix of the link computed by roll, pitch, and yaw angles. The rotation order was *Z–Y–X* from the world frame to body frame, and $\boldsymbol{E}$ is the identity matrix.

The conditions in Eqs. (6) and (7) corresponded to the preconditions. The rest of the conditions from Eqs. (8) through (13) can be described as follows.

- Eqs. (8) and (9). These conditions are mainly for the implementation on the hardware corresponding to the limitation of the angles $\theta$and the ducted-fan force F_T. In addition, the condition in Eq. (8) could help to avoid the singularities.

- Eq. (10). This condition is to prevent the robot from overturning. It mainly causes $\boldsymbol{CoM}$ to be located inside the edge support polygon. The polygon here is stricter than a general support polygon. It is defined by

the two closest edges of the projective plan of the feet (Fig. 4).

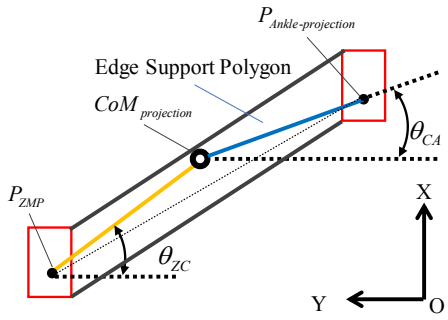

Figure 4. Projection of the robot's feet and the support polygon.

Here, θ_{ZC} is the included angle between the *Y*-axis and the connecting line of $\boldsymbol{P}_{ZMP}$ and $\boldsymbol{P}_{CoM}$, while θ_{CA} is the included angle between the *Y*-axis and the connecting line of $\boldsymbol{P}_{CoM}$ and the projective point of the swing foot's ankle $\boldsymbol{P}_{Ankle-projection}$. If $|\theta_{ZC} - \theta_{CA}|$ is large, the robot can overturn easily, because $\boldsymbol{CoM}$ is away from the edge support polygon. Although one could select a larger support polygon, the small one was chosen for the constraint because of the error on the mass model between the simulation and the real robot. Here, ρ is 5°.

- Eq. (11) is the constraint of ZMP, which can be calculated by Eqs. (1)–(3). It requires the ZMP to be located inside the support foot's polygon $\boldsymbol{S}_{foot}$. In Eq. (11), $\boldsymbol{P}_{ZMP}^{i}$ is the i^{th} step of $\boldsymbol{P}_{ZMP}$.
- Eq. (12) is the constraint from the given trajectory of the swing foot. Here, $\boldsymbol{P}_{T}^{i}$ is the position of the ducted fan determined by the position of the i^{th} step of the swing foot.
- Eq. (13) is mainly for the smoothness of the 3D stepping motion and the searching range of $\boldsymbol{P}_{body}$. The smoothness of the joint trajectory was mainly determined by the trajectory of $\boldsymbol{P}_{body}$, because of the kinematic relationship. As a result, this condition is designed to constrain the change between the current position of $\boldsymbol{P}_{body}$ and its previous position. Here, δ is a constraint and can be considered the searching range of $\boldsymbol{P}_{body}$.

C. Genetic Algorithm

As described in previous sections, there are three features in the problem and its constraint conditions: infinite solution, nonlinear items, and discrete functions. As a result, a gradient-free method would be more suitable for the problem than a gradient-based method.

The GA is a typical gradient-free method and is frequently used to search for the optimal solution in a global area. It also has solved some problems in robotics, such as inverse kinematics [12] and trajectory planning [13]. Compared with conventional methods, the main advantage of GA is that it can solve the searching or optimization problem without initial values or differentiating the equations. Additionally, the fitness function of the GA could help to avoid the need for solving complex equations. Another advantage is that its convergence has been proved [14].

D. Implementation Details of GA

There are five operations in the GA: coding, fitness function calculation, selection, crossover, and mutation. The main details and parameters for each part are as follows.

- Coding. According to the problem, the parameters of interest are $\boldsymbol{P}_{body}$ in 3D. It is performed on a string of 3 × 10 bits. Every 10 bits is assigned to P_{body-x}, P_{body-y}, and P_{body-z}, respectively. This is also performed on other operations, including selection, crossover, and mutation. Then, $\boldsymbol{P}_{body}$ can be computed from the string of 3 × 10 bits. Taking P_{body-x} as an example, it is calculated by the following:

$$P_{body-x} = \frac{x_{ub} - x_{lb}}{1023} \cdot (bit\ value) + x_{lb} \quad (14)$$

The computations of P_{body-y} and P_{body-z} are similar. Notice that $x_{\min}$ and $x_{\max}$ come from the searching range.

- Fitness function. The objective of the GA is to minimize the fitness function. First, the conditions in Eqs. (11) and (12) can be solved by generating the trajectory. Then, the problem and its constraint conditions can be translated into the form of a fitness function, which can be described as follows:

$$f = f_1 + f_2 + f_3 + f_4 \quad (15)$$

For f_1, f_2, and f_3, they can be considered as the penalty generated by the constraint conditions, and f_4 encourages the algorithm to minimize F_T when satisfying the conditions.

The item f_1 is the penalty of the posture constraint and can be described as follows.

$$f_1 = \begin{cases} 0 & \text{, if Con. (8) is true} \\ C_1 & \text{, if Con. (8) is false} \end{cases} \quad (16)$$

where C_1 is 11,000.

The item f_2 is the penalty that encourages the algorithm to cause P_{body} to be inside the edge support polygon and is as follows.

$$f_2 = \begin{cases} 0 & \text{, if Con. (10) is true} \\ C_2 & \text{, if Con. (10) is false} \end{cases} \quad (17)$$

where C_1 is 9000.

The item f_3 is also a penalty and encourages the algorithm to remain smooth, which is related to the change between the current position of P_{body} and its previous position. It can be computed by

$$f_3 = \boldsymbol{\omega}^T \cdot \Delta \quad (18)$$

where $\boldsymbol{\omega} = 50 \in \mathbb{R}^{1\times3}$ is the respective weight and $\Delta \in R^{3\times1}$ can be described as follows:

$$\Delta_x = \left(P^N_{body-x} - P^{N-1}_{body-x}\right)^2 \quad (19)$$

$$\Delta_y = \left(P^N_{body-y} - P^{N-1}_{body-y}\right)^2 \quad (20)$$

$$\Delta_z = \left(P^N_{body-z} - P^{N-1}_{body-z}\right)^2 \quad (21)$$

The item f_4 encourages the algorithm to optimize F_T to be as small as possible and can be described as follows.

$$f_4 = \begin{cases} C_{4-1} & \text{, if Con. (9) is false} \\ C_{4-2} \cdot F_T & \text{, if Con. (9) is true} \end{cases} \quad (22)$$

where C_{4-1} is 5000, and C_{4-2} is 10.

For optimization of the initial position of $\boldsymbol{P}_{body}$, the fitness function of f_3 is omitted, because the previous position of $\boldsymbol{P}_{body}$ did not exist.

- Selection, crossover, and mutation. As described above, the optimization includes two phases: the initial phase that omitted f_3 and intermediate phase that included f_3. The parameters of these two phases are different and shown in Tables 2 and 3, respectively. For the posture to be close to the global optimal posture, the searching range of the initial phase is set to be as large as possible under the robot's geometric constraint. However, the searching range of the intermediate phase is set to be small, because the available optimal position is supposed to be close to the previous position. The supposition is from the constraint of smoothness detailed in the condition in Eq. (13). The other parameters are also different in the two phases.

TABLE 2.

PARAMETERS OF GA FOR THE INITIAL PHASE

Population	200	Generation	50
$\boldsymbol{v_{min}}$	-150 (mm)	$\boldsymbol{v_{max}}$	150 (mm)
Crossover	0.5	Mutation	0.01
String length	3 × 10 bits	Fitness function	f_{init}

[a] f_{init} is fitness function omitting f_3.

TABLE 3.

PARAMETERS OF GA FOR THE INTERMEDIATE PHASE

Population	150	Generation	8
$\boldsymbol{v_{min}}$	-25 (mm)	$\boldsymbol{v_{max}}$	25 (mm)
Crossover	0.5	Mutation	0.01
String length	3 × 10 bits	Fitness function	f

IV. Simulation and Experiment

A. Balance Space

To evaluate quantitatively how the ducted-fan propulsion system improves the stepping performance of the robot, a balance space was defined. The space was the point set that the swing foot can reach under the constraint of maintaining the balance of the robot. The balance spaces in the situations with and without the propulsion system (F_T was zero) were calculated by the method of exhaustion. The result is shown in Fig. 5. The configuration and mass specification of the robot were referred to the prototype robot Jet-HR1. The maximum thrust of the ducted fan was set to be 23 N.

B. Comparison of Posture Optimization

To evaluate the effectiveness of the proposed method (GAS), including minimized thrust, smoothness of locomotion, and computational efficiency, two other algorithms were applied for comparison. The first one (called GA) was based on the proposed method but removes the fitness function of *f3* (detailed in Section III-D), which was related to the smoothness constraint. The absence of this constraint might enable the algorithm to search for the posture that needed a smaller thrust for balance. The second one

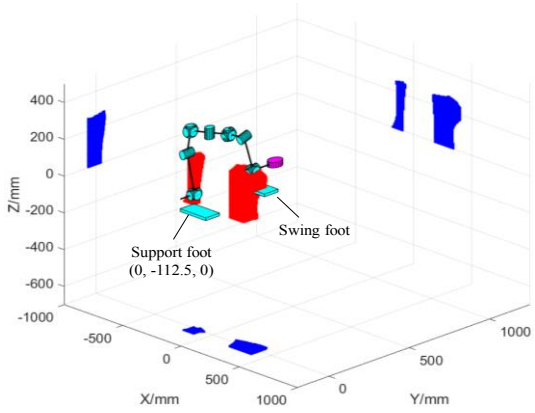

(a) Balance space without propulsion system

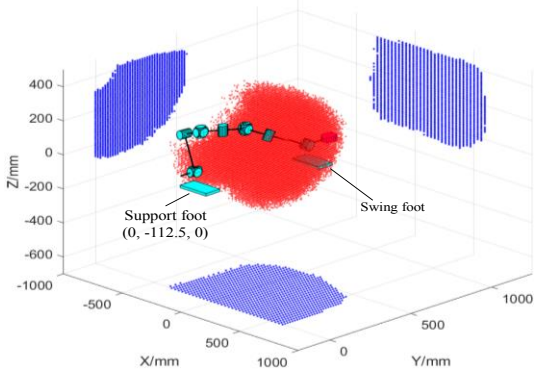

(b) Balance space with propulsion system

Figure 5. Comparison of balance space (the red point cloud represents the position that the swing foot can reach under the balance constraint).

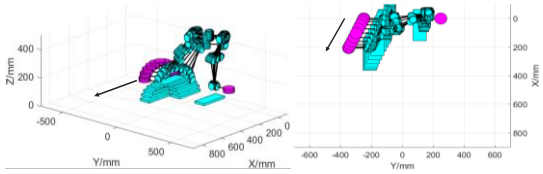

Figure 6. The locomotion of the robot during stepping to side landing point in stereo view and top view.

(GAEx) was based on the method of exhaustion. In this method, the calculation of the initial phase was the same as in the proposed method, while, for the intermediated phase, the available posture was based on local exhaustion. The searching only looks for the P_{body} satisfying the conditions without considering the minimized thrust. The methods might be beneficial for reducing the calculation time.

Two typical stepping motions were designed for the test: (1) stepping to the side and (2) stepping forward with a long-distance swing motion. A series of landing points was set to enable the robot to complete these two stepping motions in order. The trajectories of the swing foot were generated based on a circular curve. In addition, the trajectories were required to be inside the balance space described previously.

The trajectory of the swing foot of the two steps above was discretized into a series of points. Then, for each point, three methods were used to optimize the posture. For the initial phase, the parameters of the algorithms were all the same and are detailed in Table 2. For the intermediate point, the parameters of GAS and GA were the same and are detailed in Table 3. The searching range of GAEx was set as a cube with a length of 12 mm, and the searching interval was 1 mm in all axes.

The simulations were conducted and timed on the same workstation with an Intel Core i7-8700 CPU, 3.19 GHz, with 16 GB of memory, running MATLAB (version 2016b) based on Windows 10.

The result is shown in Figs. 6–9. The locomotions of the two steps using the proposed method (GAS) are shown in Figs. 6 and 8, respectively. The comparison results of the trajectories are shown in Figs. 7 and 9. In addition, Fig. 10 shows a comparison of the calculation times of the three methods.

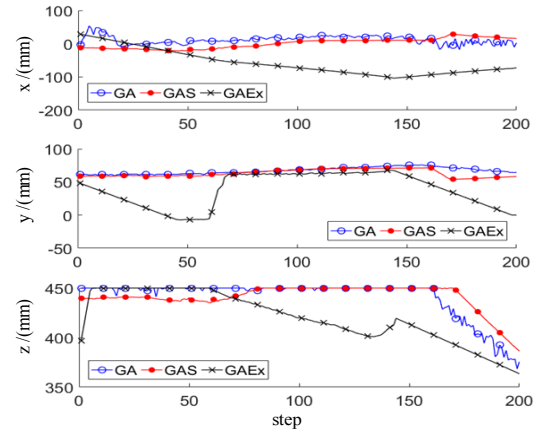

(a) Trajectory of $\boldsymbol{P_{body}}$

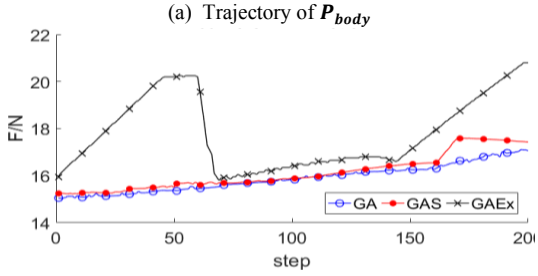

(b) Trajectory of the thrust

Figure 7. Comparison of trajectories during stepping to the side.

C. Experiment of Prototype Robot

To examine its practicability further, the calculation result of GAS in Section IV-B was applied to the prototype robot. The specification of the landing points was the same as in the simulation. All the landing points were made by carton (210 × 110 × 140 mm). During the process, the angle of each joint was according to the simulation result, while the thrust was controlled by a proportional–integral–derivative controller according to the feedback of the body's IMU. In addition, to maintain the continuity of the locomotion during double-support time, the transition motion between steps was

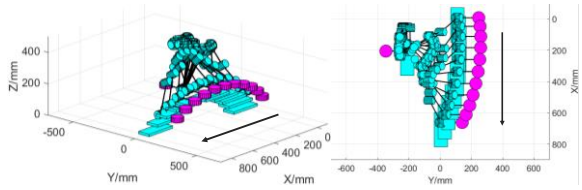

Figure 8. Locomotion of the robot during stepping forward with long distant swing motion in stereo view and top view.

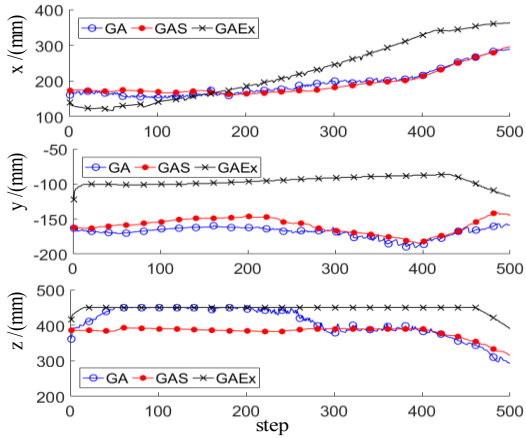

(a) Trajectory of $\boldsymbol{P_{body}}$

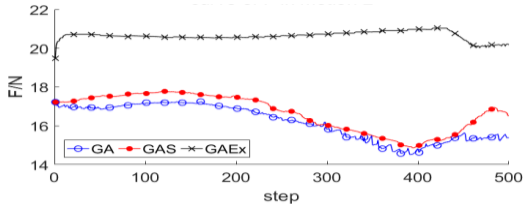

(b) Trajectory of the thrust

Figure 9. Comparison of trajectories during stepping forward with long distant swing motion.

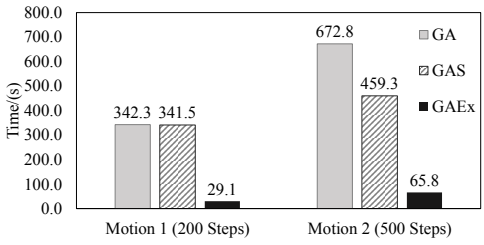

Figure 10. Comparison of calculation time.

inserted by interpolation. The experiment was repeated five times. For each trial, the robot successfully completed both steps without any intermission. The average time for each trial was 24 s. The locomotion of the robot is shown in Figs. 11.

V. Discussion and Conclusions

The results of the simulations show the effectiveness of the proposed method in solving the optimization problem. The comparison result shows that the proposed method can obtain a better balance between the minimized needed thrust and the locomotion smoothness. Compared with the GA, although the thrust generated by GAS was slightly higher, the shocks of the trajectory decreased significantly. The calculation time for GAEx was the least among the three. However, the thrust cannot be effectively optimized by GAEx and was much higher than in the proposed method.

In the experiment, the new ducted-fan propulsion system successfully enabled the prototype robot to step over a ditch by 3D stepping. During stepping with a long-distance swing motion, the thrust of the ducted fan effectively compensated for the gravity and kept the robot in quasistatic balance. The new method of posture optimization effectively minimized the thrust needed and enabled the robot to step over a ditch with a span of 450 mm (as much as 97% of the robot leg) in 3D.

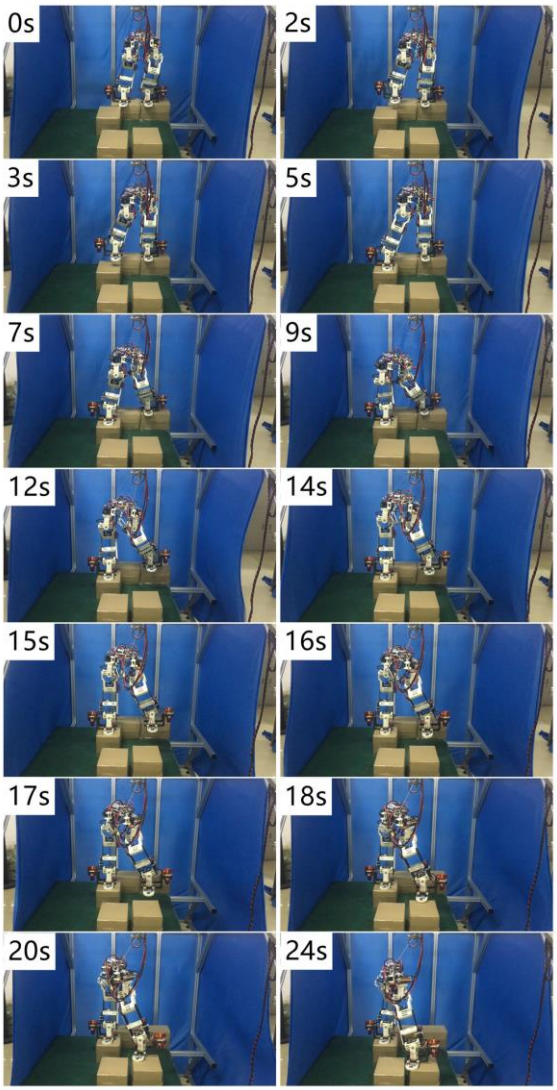

Figure 11. Motions 1 and 2 performed by Jet-HR1 (frontal view).

In future works, a focus on dynamic performance and intelligence that can enable Jet-HR1 to realize more-complex motion in various environments is planned.

References

[1] Kalamian, N., & Farrokhi, M. (2011, October). Dynamic walking of biped robots with obstacles using predictive controller. In *2011 1st International eConference on Computer and Knowledge Engineering (ICCKE)* (pp. 105-110). IEEE.

[2] Zhou, C., Wang, X., Li, Z., Caldwell, D., & Tsagarakis, N. (2015, September). Exploiting the redundancy for humanoid robots to dynamically step over a large obstacle. In *2015 IEEE/RSJ International Conference on Intelligent Robots and Systems (IROS)* (pp. 1599-1604). IEEE.

[3] Guo, F., Mei, T., Luo, M., Ceccarelli, M., Zhao, Z., Li, T., & Zhao, J. (2016). Motion planning for humanoid robot dynamically stepping over consecutive large obstacles. *Industrial Robot: An International Journal*, *43*(2), 204-220.

[4] R. J. Griffin, G. Wiedebach, S. McCrory, S. Bertrand, I. Lee and J. Pratt, "Footstep Planning for Autonomous Walking Over Rough Terrain," *2019 IEEE-RAS 19th International Conference on Humanoid Robots (Humanoids)*, Toronto, ON, Canada, 2019, pp. 9-16.

[5] Farnioli, E., Gabiccini, M., & Bicchi, A. (2016, October). Toward whole-body loco-manipulation: Experimental results on multi-contact interaction with the Walk-Man robot. In *2016 IEEE/RSJ International Conference on Intelligent Robots and Systems (IROS)* (pp. 1372-1379). IEEE.

[6] Henze, B., Ott, C., & Roa, M. A. (2014, September). Posture and balance control for humanoid robots in multi-contact scenarios based on model predictive control. In *2014 IEEE/RSJ International Conference on Intelligent Robots and Systems* (pp. 3253-3258). IEEE.

[7] Zhao, M., Anzai, T., Fan, S., Chen, X., Okada, K., & Inaba, M. (2018). Design, modeling, and control of an aerial robot dragon: a dual-rotor-embedded multilink robot with the ability of multi-degree-of-freedom aerial transformation. *IEEE Robotics & Automation Letters, 3*(2), 1176-1183.

[8] Endo, G., Hagiwara, T., Nakamura, Y., Nabae, H., & Suzumori, K. (2018, July). A proposal of super long reach articulated manipulator with gravity compensation using thrusters. In *2018 IEEE/ASME International Conference on Advanced Intelligent Mechatronics (AIM)* (pp. 1414-1419). IEEE.

[9] Pucci, D., Traversaro, S., & Nori, F. (2017). Momentum control of an underactuated flying humanoid robot. *IEEE Robotics and Automation Letters*, *3*(1), 195-202.

[10] Liu, B., Huang, Z., Wei, J., Shi, C., Ota, J., & Zhang, Y. (2018, October). Jet-HR1: Stepping Posture Optimization for Bipedal Robot Over Large Ditch Based on a Ducted-fan Propulsion System. In *2018 IEEE/RSJ International Conference on Intelligent Robots and Systems (IROS)* (pp. 6010-6015). IEEE.

[11] S. Kajita, H. Hirukawa, K. Harada, et al., "Introduction to humanoid robotics," *Springer Berlin Heidelberg,* 2014.

[12] Yang, Y., Peng, G., Wang, Y., & Zhang, H. (2007, August). A new solution for inverse kinematics of 7-DOF manipulator based on genetic algorithm. In *2007 IEEE International Conference on Automation and Logistics* (pp. 1947-1951). IEEE.

[13] Van-Huan, D., Chew, C. M., & Poo, A. N. (2008, September). Optimized joint-torques trajectory planning for bipedal walking robots. In *2008 IEEE Conference on Robotics, Automation and Mechatronics* (pp. 1142-1147). IEEE.

[14] Greenhalgh, D., & Marshall, S. (2000). Convergence criteria for genetic algorithms. *SIAM Journal on Computing*, *30*(1), 269-282.